

State-resolved multimodal contributions to stratospheric polar vortex predictability

Shuo Yang^{*1,2}, Dan Zhao^{*1,2}, Tingting Xue^{1,2}, Chunhua Zeng^{1,2}, Yongwen Zhang^{†1,2}, and Xiaosong Chen^{†,3}

¹Yunnan Key Laboratory of Complex Systems and Brain-Inspired Intelligence, Kunming University of Science and Technology, Kunming 650500, Yunnan, China

²Faculty of Science, Kunming University of Science and Technology, Kunming 650500, Yunnan, China

³Institute for Advanced Study in Physics and School of Physics, Zhejiang University, Hangzhou 310058, China

Abstract

The dynamical basis of stratospheric polar vortex predictability remains unclear, particularly the relative roles of persistence, structural variability, and cross-level coupling. Here we provide a state-resolved and quantitative framework using eigen microstate theory applied to ERA5 geopotential height fields, enabling attribution of predictability to dynamically coherent circulation states via a mesoscopic Granger-causality approach. We show that short-term predictability is dominated by persistence of the leading stratospheric state, whereas extended predictability arises from higher-order stratospheric structures and tropospheric variability. These contributions exhibit strong lead-time dependence and become more distributed during sudden stratospheric warming events. Our results unify SPV predictability within a multimodal, state-resolved framework and provide a physically interpretable pathway for improving subseasonal-to-seasonal forecasts.

1 Introduction

The stratospheric polar vortex (SPV) is a major source of subseasonal-to-seasonal predictability in the Northern Hemisphere, exerting a strong influence on midlatitude weather through downward coupling to the troposphere [1, 2]. This downward influence modulates large-scale circulation patterns such as the Arctic Oscillation and Northern Annular Mode [3–5], with important impacts on surface climate variability and extreme events [2, 6].

*These authors contributed equally to this work.

†Corresponding authors: zhangyongwen77@gmail.com (Y.Z.), chenxs@zju.edu.cn (X.C.)

Despite substantial progress in characterizing its variability and impacts, a fundamental question remains unresolved: what determines the dynamical origin of SPV predictability? While enhanced forecast skill is often linked to the persistence of the vortex [7–9], the extratropical stratosphere also exhibits extended predictability relative to the troposphere [10]. It therefore remains unclear whether SPV predictability arises primarily from this bulk memory or from more complex interactions among multiple circulation structures.

Previous studies have identified key dynamical processes governing SPV variability, including planetary wave propagation and wave–mean-flow interaction, which control both the strength and structure of the vortex [11–13]. In particular, strong upward-propagating Rossby waves from the troposphere can perturb and even disrupt the vortex, leading to sudden stratospheric warming (SSW) events [13–15]. In addition, stratosphere–troposphere coupling has been recognized as a major pathway through which stratospheric variability influences surface climate and enhances subseasonal predictability [2, 6, 16].

From a statistical perspective, dominant variability is often characterized using EOF- or PCA-based methods [17–19], and predictive relationships are explored using regression-based or data-driven approaches [20, 21]. However, these approaches typically rely on low-dimensional representations or leading modes and do not explicitly quantify how multiple circulation states jointly contribute to predictability across timescales and dynamical regimes. In particular, it remains unclear whether extended-range predictability emerges primarily from a single dominant mode or from the collective contribution of multiple interacting states, and how this balance may shift between normal winters and winters with SSWs, which are known to exhibit distinct dynamical evolution and predictability characteristics [22, 23].

Here we propose that SPV predictability has a fundamentally multimodal dynamical origin, arising from the joint evolution of multiple stratospheric and tropospheric states. To test this hypothesis, we adopt Eigen Microstate Theory (EMT), first introduced by [24, 25], and later extended to nonequilibrium systems and climate prediction problems, including the increased predictability of extreme El Niño from decadal interbasin interaction [26, 27]. We further combine EMT with a Granger-causality framework, in which causality is defined at the level of eigen microstates rather than individual variables [28, 29]. This mesoscopic representation captures dynamically coherent circulation structures and enables us to quantify how distinct circulation states govern the evolution and predictability of the system. Using ERA5 data (1948–2023), we show that short-range predictability is dominated by persistence of the leading stratospheric state, whereas longer-range predictability emerges from additional stratospheric and tropospheric states through cross-level coupling. This multimodal organization is strongly state dependent, with enhanced contributions from higher-order states during SSW winters.

2 Data and Methods

2.1 Data and preprocessing

We analyze geopotential height fields from the ERA5 reanalysis at 10 hPa and 500 hPa, representing the stratospheric and tropospheric circulation, respectively [30]. The analysis domain is the Arctic polar cap (65°–90°N) on a $2.5^\circ \times 2.5^\circ$ grid, and the study period spans 1948–2023. Daily mean fields are computed from 6-hourly data. To isolate subseasonal variability, a multi-year daily climatology is removed at each grid point, yielding

deseasonalized anomaly fields. We denote the anomaly fields at time t as $\mathbf{x}^S(t)$ and $\mathbf{x}^T(t)$, representing the stratospheric (10 hPa) and tropospheric (500 hPa) circulation, respectively.

The SPV index is defined as the normalized polar-cap-averaged geopotential height anomaly at 10 hPa, with monthly linear trends removed prior to normalization[31]. Winters are classified as SSW winters or normal winters based on the reversal of zonal-mean zonal wind at 10 hPa and 60°N[32]. We focus on SPV variability during the extended winter season from November to April. To construct predictors with sufficient lead time, data from September to April are additionally used, allowing up to 60 days of prior information to be included in the analysis.

2.2 Eigen-microstate decomposition

To extract dominant circulation structures, we apply EMT separately to the stratosphere and troposphere.

For each layer, the EMT decomposition is performed over the concatenated seasonal segments from September of each year to April of the following year across all winters.

For the stratosphere, anomaly fields are assembled into an ensemble matrix[24, 25]:

$$\mathbf{Z}^S = [\mathbf{x}^S(t_1) - \bar{\mathbf{x}}^S, \dots, \mathbf{x}^S(t_M) - \bar{\mathbf{x}}^S], \quad (1)$$

where

$$\bar{\mathbf{x}}^S = \frac{1}{M} \sum_{m=1}^M \mathbf{x}^S(t_m) \quad (2)$$

is the time mean over the full sampled period.

We normalize the ensemble matrix using the Frobenius norm,

$$\tilde{\mathbf{Z}}^S = \frac{\mathbf{Z}^S}{\|\mathbf{Z}^S\|_F}, \quad (3)$$

where $\|\cdot\|_F$ denotes the Frobenius norm.

Singular value decomposition (SVD) is then applied:

$$\tilde{\mathbf{Z}}^S = \mathbf{U}^S \boldsymbol{\Sigma}^S (\mathbf{V}^S)^\top. \quad (4)$$

For the stratosphere, we denote the i th eigen microstate by S_i , whose temporal coefficient $a_i^S(t)$ is given by the (t, i) element of \mathbf{V}^S , and whose spatial pattern is given by the i th column of \mathbf{U}^S . Similarly, for the troposphere, we obtain eigen microstates T_i with temporal coefficients $a_i^T(t)$, where the spatial patterns are given by the columns of \mathbf{U}^T .

The contribution of each state is quantified by

$$p_i^X = (\sigma_i^X)^2, \quad X \in \{S, T\}, \quad (5)$$

which represents the fraction of variance explained by each mode.

2.3 Identification of SPV-related states

We next identify which circulation states are most relevant to SPV variability.

For each state, we compute the lagged correlation between its temporal coefficient and the SPV index:

$$r_i^X(\tau) = \text{corr}(a_i^X(t - \tau), \text{SPV}(t)), \quad (6)$$

where $\tau \geq 0$ denotes the lag, and t is restricted to the period from November to April.

For each state, we identify the lag that maximizes the absolute correlation for $\tau \geq 0$:

$$\tau_i^* = \arg \max_{\tau \in [0, \tau_{\max}]} |r_i^X(\tau)|, \quad (7)$$

and define the predictive relevance as

$$R_i^X = r_i^X(\tau_i^*), \quad (8)$$

where $\tau_{\max} = 60$ days.

Statistical significance is assessed using phase-randomized surrogate data. States exceeding the 95% confidence level are retained. Based on this criterion, we select the related stratospheric states and tropospheric states.

2.4 Prediction framework

To quantify the predictive contribution of circulation states, we adopt a Granger-causal autoregressive framework[28].

Because the leading stratospheric state is highly correlated with the SPV index (see Supporting Information Figure S1), we define the prediction target as

$$z(t) = a_1^S(t). \quad (9)$$

Baseline model:

$$z(t+1) = c + \sum_{\tau=0}^{\tau_{\max}-1} \alpha_{\tau} z(t-\tau) + \epsilon_t^{(B)}. \quad (10)$$

Multimodal model:

Let \mathcal{S} and \mathcal{T} denote the sets of selected stratospheric and tropospheric states, respectively. Since the leading stratospheric state is used as the prediction target in Eq. (9), it is excluded from the stratospheric predictor set on the right-hand side. The one-step multimodal model is written as

$$\begin{aligned} z(t+1) = c &+ \sum_{\tau=0}^{\tau_{\max}-1} \alpha_{\tau} z(t-\tau) \\ &+ \sum_{\tau=0}^{\tau_{\max}-1} \sum_{i \in \mathcal{S}} \beta_{\tau,i} a_i^S(t-\tau) \\ &+ \sum_{\tau=0}^{\tau_{\max}-1} \sum_{j \in \mathcal{T}} \gamma_{\tau,j} a_j^T(t-\tau) + \epsilon_t^{(M)}, \end{aligned} \quad (11)$$

where \mathcal{S} contains the selected stratospheric states excluding the leading states, and \mathcal{T} contains the selected tropospheric states. Once the one-step model (10)–(11) is fitted, multi-step forecasts are generated iteratively.

2.5 Predictability and Granger causality

Predictability at lead time h is quantified by the Pearson correlation:

$$\text{Skill}(h) = \text{corr}(z_{\text{pred}}^{(h)}(t), z_{\text{obs}}(t+h)), \quad (12)$$

where $z_{\text{pred}}^{(h)}(t)$ denotes the h -step-ahead prediction initialized at time t .

Predictability is evaluated separately for all winters, SSW winters, and normal winters by restricting the verification samples to the corresponding subsets.

To quantify the contribution of each selected eigen microstate to predictability, we construct a Granger-causal framework based on the multimodal model in Eq. (11). Specifically, for each selected eigen microstate, we compare the full model with a reduced model in which the corresponding state is excluded.

For a given eigen microstate i , the residuals of the full model are defined as

$$e_h^{(\text{full})}(t) = z_{\text{obs}}(t+h) - z_{\text{pred}}^{(h)}(t), \quad (13)$$

and the residuals of the reduced model (excluding state i) are defined as

$$e_h^{(-i)}(t) = z_{\text{obs}}(t+h) - z_{\text{pred},-i}^{(h)}(t), \quad (14)$$

where $z_{\text{pred},-i}^{(h)}(t)$ denotes the prediction obtained from the model with the i th eigen microstate removed from Eq. (11).

The corresponding residual sums of squares are given by

$$RSS_{\text{full}}^{(h)} = \sum_t \left(e_h^{(\text{full})}(t) \right)^2, \quad RSS_{-i}^{(h)} = \sum_t \left(e_h^{(-i)}(t) \right)^2. \quad (15)$$

The F-statistic for assessing the contribution of the i th eigen microstate is then defined as

$$F_{i,h} = \frac{(RSS_{-i}^{(h)} - RSS_{\text{full}}^{(h)})/d_i}{RSS_{\text{full}}^{(h)}/(n_h - d_{\text{full}})}, \quad (16)$$

where d_i is the number of parameters associated with the i th eigen microstate in Eq. (11), d_{full} is the total number of parameters in the full model, and n_h is the sample size for lead time h .

A significant $F_{i,h}$ indicates that removing the i th eigen microstate leads to a statistically significant degradation in predictive skill, implying that this state provides independent predictive information. In this sense, each eigen microstate is said to exhibit Granger causality with respect to the SPV at lead time h . After obtaining $F_{i,h}$, the corresponding p -value is computed from the F distribution with appropriate degrees of freedom. Typically, when $p < 0.05$, the contribution of the i th eigen microstate is considered statistically significant.

3 Results

3.1 Eigen microstates associated with SPV variability

We first apply EMT to the stratosphere and troposphere using all winters from 1948 to 2023 (see Section 2.2), focusing on the polar-cap domain (65° – 90° N). Using the lagged-correlation framework defined in Eq. (6), we quantify the relationship between each eigen

microstate and the SPV index. Supplementary Fig. S1 shows examples of the lagged-correlation functions for representative stratospheric eigen microstates. The leading state S_1 is nearly identical to the SPV index, exhibiting a maximum correlation of 0.994 at zero lag (Supplementary Fig. S1a), confirming that it captures the bulk variability of the polar vortex. In contrast, higher-order states exhibit asymmetric lagged-correlation structures with extrema at nonzero lags (e.g., S_2 in Supplementary Fig. S1b), indicating potential predictive relationships with subsequent SPV evolution.

To systematically identify eigen microstates with predictive relevance, we compute R_i^S (Eq. (8)) for all stratospheric eigen microstates. Figure 1a shows R_i^S for the leading 100 eigen microstates together with the 95% confidence interval. The leading states S_1 , S_2 , S_3 , and S_6 exceed the significance threshold. Although S_4 and S_5 do not pass the significance test, they possess relatively large eigenvalues and are therefore retained to preserve the dominant variance-contributing structures. As a result, six leading stratospheric eigen microstates (S_1 – S_6) are selected for subsequent analysis.

Figures 1b–g show the spatial patterns of these states over the polar cap. The leading mode S_1 exhibits a nearly axisymmetric monopole structure (Fig. 1b), representing coherent strengthening and weakening of the vortex consistent with previous studies in which the dominant winter stratospheric variability is primarily associated with changes in polar-vortex intensity [33]. This state reflects the intrinsic memory of the SPV and corresponds to variability in its bulk intensity.

The next pair, S_2 and S_3 , displays dipolar structures (Figs. 1c and d) and forms an approximately orthogonal pair. These modes represent large-scale zonal asymmetry within the polar cap and correspond to two rotated realizations of vortex displacement. Their structure is consistent with wave-1-type perturbations, which are known to shift the vortex away from the pole and reorganize its horizontal position [34, 35]. The following pair, S_4 and S_5 , exhibits quadrupolar structures (Figs. 1e and f), again forming an approximately orthogonal pair. These modes represent more complex deformation of the vortex edge, with alternating centers of opposite sign across the polar cap. Their structure is consistent with wave-2-type disturbances and is indicative of split-prone vortex configurations and enhanced structural heterogeneity [36].

The higher-order state S_6 exhibits a polar-centered structure (Fig. 1g). This state resembles a radially structured higher-order monopole, reflecting variability in the radial structure and confinement of the vortex rather than its horizontal displacement or deformation. To further examine a large-scale context, we also compute the spatial patterns over the entire Northern Hemisphere (NH), as shown in Supplementary Fig. S2. The dominant structures remain concentrated within the polar cap and exhibit patterns consistent with those in Fig. 1.

A similar analysis for the troposphere identifies seven dominant eigen microstates (Fig. 2). Consistent with their dynamical role, the lagged-correlation functions of the tropospheric eigen microstates (Supplementary Fig. S3) exhibit maxima at nonzero lags, indicating that tropospheric variability typically precedes changes in the SPV. However, their correlations are generally weaker than those of the stratospheric eigen microstates.

Compared to the stratospheric states, the tropospheric eigen microstates exhibit stronger spatial asymmetry and more complex multipolar structures, which are more clearly revealed in the NH patterns shown in Supplementary Fig. S4. These structures resemble large-scale Rossby wave trains and teleconnection patterns extending from the midlatitudes into the polar region, reflecting the influence of midlatitude wave activity on polar circulation [37]. This suggests that tropospheric state primarily acts as a source

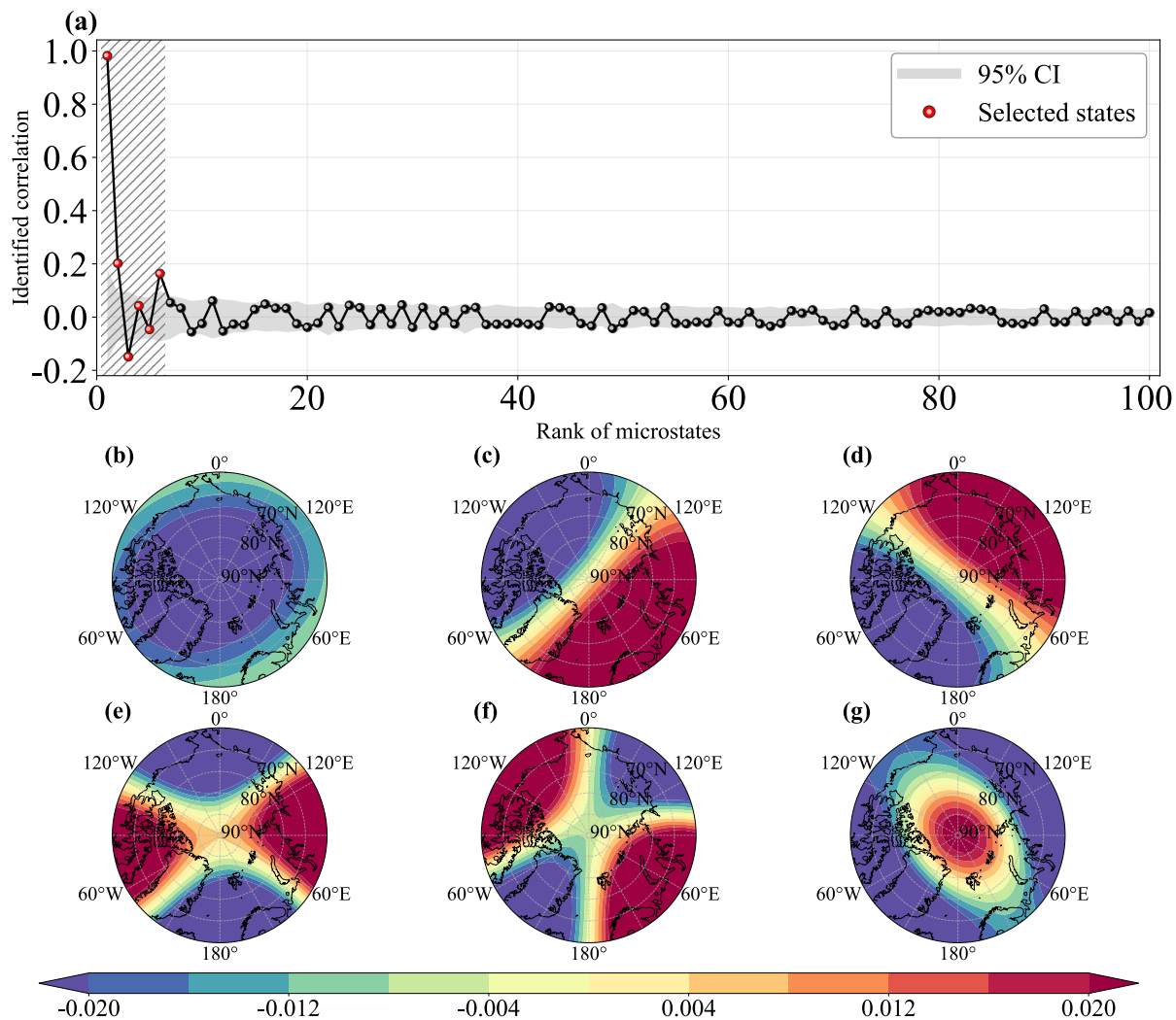


Figure 1: Predictive relevance and spatial patterns of the selected stratospheric eigen microstates. (a) The identified correlation R_i^S (Eq. (8)) for the first 100 eigen microstates. Red dots represent the selected eigen microstates. The shaded region indicates the 95% confidence intervals estimated from surrogate data. (b–g) Spatial patterns of the six selected stratospheric eigen microstates at 10 hPa. The contributions of each state correspond to S_1 – S_6 with 71.82%, 13.33%, 8.98%, 1.77%, 1.55%, and 1.47%, respectively.

of dynamical forcing, modulating the SPV rather than directly determining its state.

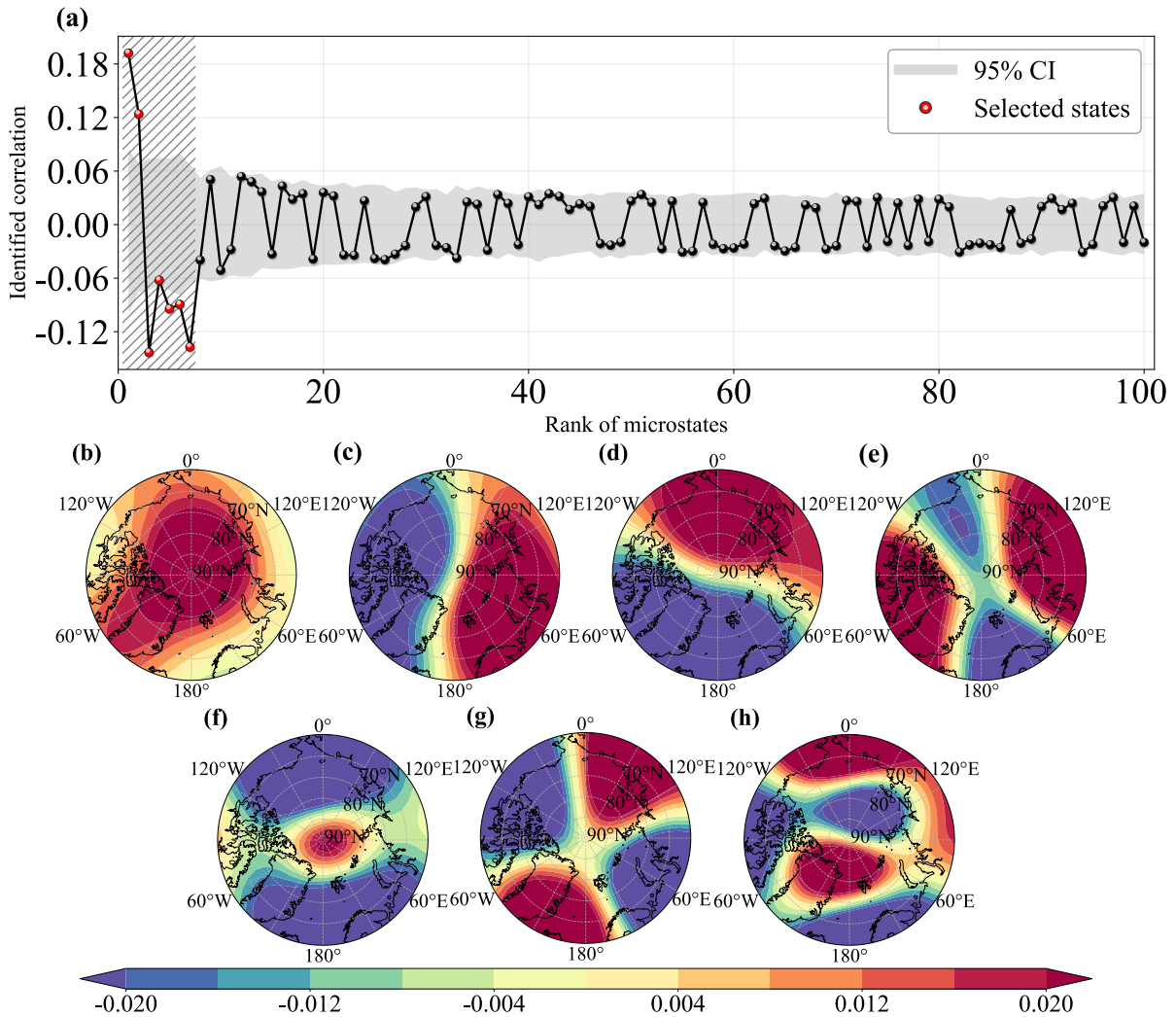


Figure 2: Predictive relevance and spatial patterns of the selected tropospheric eigen microstates. (a) The identified correlation R_i^T for the first 100 eigen microstates. (b–h) Spatial patterns of the seven selected tropospheric eigen microstates at 500 hPa. The contributions of each state correspond to T_1 – T_7 with 35.39%, 14.52%, 10.19%, 7.11%, 6.64%, 5.37%, and 2.74%, respectively.

3.2 Multimodal contributions to SPV predictability

We next assess how the selected eigen microstates contribute to SPV predictability as a function of lead time. Figure 3 compares prediction correlations under different model configurations. A restricted baseline model, relying solely on the autoregressive memory of the leading stratospheric state S_1 , exhibits a rapid decay in forecast correlation with increasing lead time (Fig. 3a). At short lead times, the model retains relatively high skill, reflecting the intrinsic persistence of the bulk vortex-intensity mode. However, this skill decreases substantially at longer lead times, indicating that persistence alone is insufficient to sustain extended-range predictability.

This behavior depends on the dynamical regime. During normal winters, the baseline model retains modest skill at intermediate lead times, consistent with the relatively

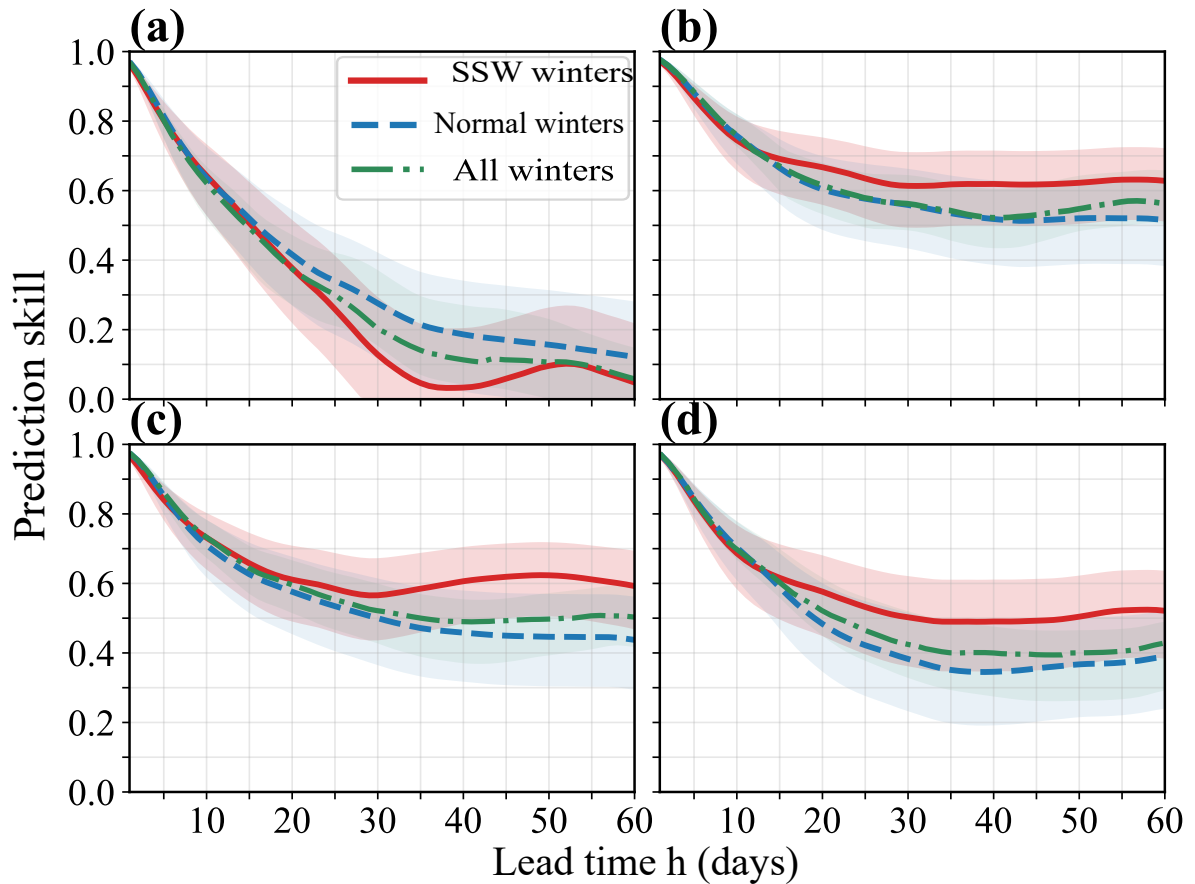


Figure 3: Prediction skill measured by correlation (Eq. (12)) as a function of lead time for different model configurations and winter regimes. Shading indicates the corresponding confidence intervals. (a) Baseline model including only the leading stratospheric eigen microstate S_1 . (b) Full multimodal model (Eq. (11)) including all selected stratospheric (S_1 – S_6) and tropospheric (T_1 – T_7) eigen microstates. (c) Model including only stratospheric states (S_1 – S_6). (d) Model including S_1 together with all tropospheric states (T_1 – T_7).

stable and near-axisymmetric vortex structure. In contrast, during SSW winters, forecast correlations decrease much more rapidly after approximately one month (Fig. 3a), indicating that persistence of S_1 alone fails to capture vortex evolution under strongly disturbed conditions. The all-winters result lies between these two regimes, reflecting an average response across different dynamical states.

In contrast, incorporating the full multimodal structure, by including both stratospheric and tropospheric eigen microstates (Eq. (11)), substantially improves prediction skill (Fig. 3b). The extended model maintains significantly higher correlations at medium and long lead times and slows the decay of predictability. This improvement is particularly pronounced during SSW winters, for which the multimodal model preserves relatively high skill at longer leads. For example, at a representative lead time of 30 days, the multimodal model increases forecast skill by approximately 346% during SSW winters and 103% during normal winters relative to the baseline. During normal winters, the gain is smaller but still systematic, as persistence already provides a more stable baseline. For all winters combined, the extended model exhibits consistently enhanced and smoother skill across lead times, indicating that multimodal coupled variability provides a robust source of predictability.

To further disentangle the sources of this improvement, we separately evaluate the contributions from stratospheric and tropospheric states. When only additional stratospheric states (S_2 – S_6) are included (Fig. 3c), the model shows a clear and systematic increase in forecast skill across most lead times. This enhancement is particularly evident during SSW winters. At 30-day lead time, the inclusion of stratospheric structural states leads to an improvement of approximately 323% for SSW winters and 81% for normal winters relative to the baseline, highlighting the dominant role of internal vortex-structure variability.

Including only tropospheric states (T_1 – T_7) also improves forecast skill (Fig. 3d), although the magnitude of improvement is smaller. At the same lead time, the contribution from tropospheric states corresponds to an increase of approximately 266% during SSW winters and 39% during normal winters. For the all-winters sample, tropospheric states provide additional predictive information, but their contribution remains weaker than that of the internal stratospheric states. This indicates that tropospheric variability contributes to SPV predictability through cross-level dynamical coupling, but its independent contribution is secondary to that of the intrinsic stratospheric structure.

3.3 Granger causality of multimodal predictability

To further quantify the dynamical contributions of individual circulation states, we analyze both the regression coefficients and the Granger-causal significance associated with each eigen microstate using the framework defined in Eq. (16). The regression coefficients (α , β , γ) correspond to the contributions of the leading stratospheric state, higher-order stratospheric states, and tropospheric states defined in Eq. (11), respectively. Figure 4 summarizes these results for all winters, SSW winters, and normal winters.

For all winters (Figs. 4a,d), the leading stratospheric state S_1 exhibits the largest regression coefficients (α) at short lead times, consistent with its dominant role in short-term predictability. However, its contribution decreases with increasing lead time. In contrast, higher-order stratospheric states (S_2 and S_3) show peak contributions at intermediate lead times (approximately 20–30 days), reflected in enhanced coefficients (β), indicating that vortex structural variability becomes increasingly important for extended prediction.

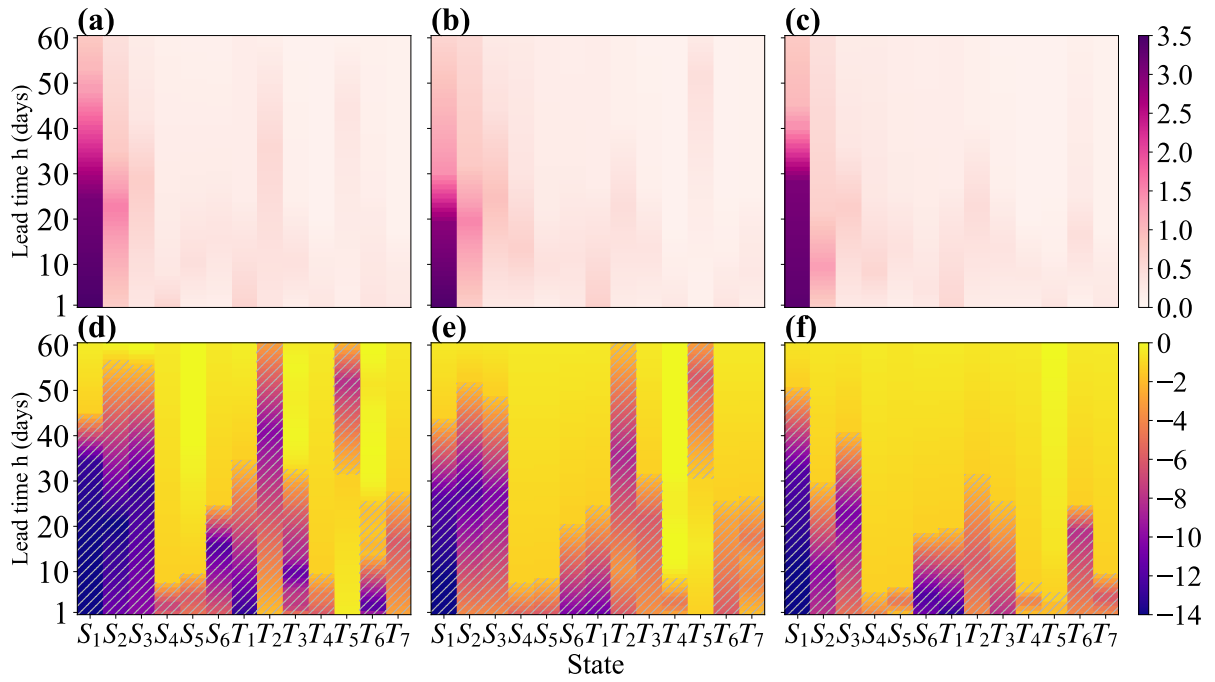


Figure 4: Regression coefficients and Granger-causality significance as a function of lead time for individual eigen microstates. (a–c) Regression coefficient magnitude associated with each state for all winters, SSW winters, and normal winters, respectively. (d–f) Corresponding Granger-causality significance (p-values) based on Eq. (16), expressed as $\log_{10}(p)$, where more negative values indicate stronger statistical significance. Regions with $p \leq 0.05$ are indicated by diagonal hatching.

This transition is accompanied by enhanced Granger-causal significance (Fig. 4d), confirming that these states provide independent predictive information beyond the leading mode.

Tropospheric states, associated with coefficients (γ), exhibit weaker amplitudes overall (Fig. 4a), but several states show statistically significant Granger-causal contributions at intermediate and longer lead times (Fig. 4d). Combined with their nonzero lag correlations (Section 3.1), this indicates that tropospheric variability contributes to SPV predictability through cross-level dynamical coupling, acting as a source of external forcing rather than direct control.

The causal structure differs markedly between dynamical regimes. During SSW winters (Figs. 4b,e), multiple stratospheric and tropospheric states exhibit enhanced regression coefficients and strong Granger-causal significance across a broad range of lead times. In particular, higher-order stratospheric states and several tropospheric modes remain significant at longer lead times, indicating that predictability arises from the interaction of multiple dynamically evolving structures under strongly forced conditions. In contrast, during normal winters (Figs. 4c,f), the dominant contribution is largely confined to the leading stratospheric state S_1 , with less persistent contributions from higher-order states. The corresponding Granger-causal significance is also more localized in lead time, reflecting a system closer to a stable background state with limited structural variability.

4 Conclusion

In this study, we provide a state-resolved and quantitative framework for understanding the predictability of SPV based on EMT and mesoscopic Granger-causality analysis. By decomposing atmospheric circulation into dynamically coherent states, we identify how both internal stratospheric variability and tropospheric forcing contribute to SPV evolution.

Our results show that SPV variability is characterized by a hierarchy of stratospheric eigen microstates, ranging from the leading state representing bulk vortex intensity to higher-order states associated with displacement, deformation, and structural reorganization. In contrast, tropospheric eigen microstates exhibit wave-train-like structures and act as precursors that influence the stratosphere. We demonstrate that SPV predictability is inherently multimodal and strongly lead-time dependent. Short-term predictability is primarily governed by the persistence of the leading stratospheric state, reflecting the intrinsic memory of the vortex. At longer lead times, predictability emerges from the combined contributions of higher-order stratospheric states and tropospheric forcing, indicating that structural variability and cross-level interactions provide predictive information beyond bulk vortex intensity.

Furthermore, the causal structure of predictability depends strongly on the dynamical regime. During SSW winters, predictability is governed by a broader set of interacting states, whereas during normal winters it is largely dominated by a single leading mode.

Together, these results demonstrate that SPV predictability is inherently multimodal and can be quantitatively characterized within a unified, state-resolved framework. This approach extends predictability analysis beyond traditional low-dimensional indices and provides a physically interpretable pathway for improving subseasonal-to-seasonal forecasts.

Open Research Section

The ERA5 geopotential height data on pressure levels used in this study [30] are publicly available from the Copernicus Climate Change Service (C3S) Climate Data Store (CDS).

Conflict of Interest Declaration

The authors declare there are no conflicts of interest for this study.

Acknowledgments

We thank the National Key Research and Development Program of China (Grant No. 2023YFE0109000) and the National Natural Science Foundation of China (Grants No. 12305044 and No. 12135003) for financial support.

References

- [1] Mark P. Baldwin and Timothy J. Dunkerton. Stratospheric harbingers of anomalous weather regimes. *Science*, 294(5542):581–584, 2001. doi: 10.1126/science.1063315.
- [2] Daniela I. V. Domeisen, Amy H. Butler, Andrew Charlton-Perez, Belén Ayarzagüena, Mark P. Baldwin, Etienne Dunn-Sigouin, Jason C. Furtado, Chaim I. Garfinkel, Peter Hitchcock, Alexey Y. Karpechko, Hye-Mi Kim, Jeff Knight, Amy L. Lang, Eun-Pa Lim, Andrew Marshall, George Roff, Chen Schwartz, Isla R. Simpson, Seok-Woo Son, and Masakazu Taguchi. The role of the stratosphere in subseasonal to seasonal prediction: 2. predictability arising from stratosphere–troposphere coupling. *Journal of Geophysical Research: Atmospheres*, 125(2):e2019JD030923, 2020. doi: 10.1029/2019JD030923.
- [3] Mark P. Baldwin and Timothy J. Dunkerton. Propagation of the arctic oscillation from the stratosphere to the troposphere. *Journal of Geophysical Research: Atmospheres*, 104(D24):30937–30946, 1999. doi: 10.1029/1999JD900445.
- [4] David W. J. Thompson and John M. Wallace. Annular modes in the extratropical circulation. part i: Month-to-month variability. *Journal of Climate*, 13(5):1000–1016, 2000. doi: 10.1175/1520-0442(2000)013<1000:AMITEC>2.0.CO;2.
- [5] David W. J. Thompson, John M. Wallace, and Gabriele C. Hegerl. Annular modes in the extratropical circulation. part ii: Trends. *Journal of Climate*, 13(5):1018–1036, 2000.
- [6] Joseph Kidston, Adam A. Scaife, Steven C. Hardiman, Daniel M. Mitchell, Neal Butchart, Mark P. Baldwin, and Lesley J. Gray. Stratospheric influence on tropospheric jet streams, storm tracks and surface weather. *Nature Geoscience*, 8(6):433–440, 2015. doi: 10.1038/NGEO2424.
- [7] Adam A. Scaife, Alberto Arribas, Edward Blockley, Adrian Brookshaw, Richard T. Clark, Nick Dunstone, Rosie Eade, Dave Fereday, Chris K. Folland, Matthew Gordon, Leon Hermanson, Jeff R. Knight, Daniel J. Lea, Craig MacLachlan, Anna

- Maidens, Matthew Martin, Kate A. Peterson, Doug Smith, Michael Vellinga, Emily Wallace, Jason Waters, and Adam Williams. Skillful long-range prediction of european and north american winters. *Geophysical Research Letters*, 41(7):2514–2519, 2014. doi: 10.1002/2014GL059637.
- [8] Om P. Tripathi, Andrew Charlton-Perez, Michael Sigmond, and Frederic Vitart. Enhanced long-range forecast skill in boreal winter following stratospheric strong vortex conditions. *Environmental Research Letters*, 10(10):104007, 2015. doi: 10.1088/1748-9326/10/10/104007.
- [9] Jadwiga H. Richter, Kathy Pegion, Lantao Sun, Hyemi Kim, Julie M. Caron, Anne Glanville, Emerson LaJoie, Stephen Yeager, Who M. Kim, Ahmed Tawfik, and D. Collins. Subseasonal prediction with and without a well-represented stratosphere in cesm1. *Weather and Forecasting*, 35:2589–2602, 2020. doi: 10.1175/WAF-D-20-0029.1.
- [10] Daniela I. V. Domeisen, Amy H. Butler, Andrew Charlton-Perez, Belén Ayarzagüena, Mark P. Baldwin, Etienne Dunn-Sigouin, Jason C. Furtado, Chaim I. Garfinkel, Peter Hitchcock, Alexey Y. Karpechko, Hye-Mi Kim, Jeff Knight, Amy L. Lang, Eun-Pa Lim, Andrew Marshall, George Roff, Chen Schwartz, Isla R. Simpson, Seok-Woo Son, and Masakazu Taguchi. The role of the stratosphere in subseasonal to seasonal prediction: 1. predictability of the stratosphere. *Journal of Geophysical Research: Atmospheres*, 125(2):e2019JD030920, 2020. doi: 10.1029/2019JD030920.
- [11] Jule G. Charney and Philip G. Drazin. Propagation of planetary-scale disturbances from the lower into the upper atmosphere. *Journal of Geophysical Research*, 66(1):83–109, 1961. doi: 10.1029/JZ066i001p00083.
- [12] James R. Holton and Clifford Mass. Stratospheric vacillation cycles. *Journal of the Atmospheric Sciences*, 33(11):2218–2225, 1976. doi: 10.1175/1520-0469(1976)033<2218:SVC>2.0.CO;2.
- [13] Taroh Matsuno. A dynamical model of the stratospheric sudden warming. *Journal of the Atmospheric Sciences*, 28(8):1479–1494, 1971. doi: 10.1175/1520-0469(1971)028<1479:ADMOTS>2.0.CO;2.
- [14] Amy H. Butler, Dian J. Seidel, Steven C. Hardiman, Neal Butchart, Thomas Birner, and Aaron Match. Defining sudden stratospheric warmings. *Bulletin of the American Meteorological Society*, 96(11):1913–1928, 2015. doi: 10.1175/BAMS-D-13-00173.1.
- [15] Mark P Baldwin, Blanca Ayarzagüena, Thomas Birner, Neal Butchart, Amy H Butler, Andrew J Charlton-Perez, Daniela IV Domeisen, Chaim I Garfinkel, Hella Garny, and Edwin P Gerber. Sudden stratospheric warmings. *Reviews of Geophysics*, 59(1):e2020RG000708, 2021.
- [16] Amy Butler, Andrew Charlton-Perez, Daniela I. V. Domeisen, Chaim Garfinkel, Edwin P. Gerber, Peter Hitchcock, Alexey Y. Karpechko, Amanda C. Maycock, Michael Sigmond, Isla Simpson, and Seok-Woo Son. Sub-seasonal predictability and the stratosphere. In Andrew W. Robertson and Frederic Vitart, editors, *Sub-seasonal to Seasonal Prediction: The Gap Between Weather and Climate Forecasting*, pages 223–241. Elsevier, Amsterdam, 2018. doi: 10.1016/B978-0-12-811714-9.00011-5.

- [17] Abdel Hannachi, Ian T. Jolliffe, and David B. Stephenson. Empirical orthogonal functions and related techniques in atmospheric science: A review. *International Journal of Climatology*, 27(9):1119–1152, 2007. doi: 10.1002/joc.1499.
- [18] Ian T. Jolliffe. *Principal Component Analysis*. Springer, New York, 2 edition, 2002.
- [19] Adam H. Monahan, John C. Fyfe, Maarten H. P. Ambaum, David B. Stephenson, and Gerald R. North. Empirical orthogonal functions: The medium is the message. *Journal of Climate*, 22(24):6501–6514, 2009. doi: 10.1175/2009JCLI3062.1.
- [20] Marlene Kretschmer, Jakob Runge, and Dim Coumou. Early prediction of extreme stratospheric polar vortex states based on causal precursors. *Geophysical Research Letters*, 44(16):8592–8600, 2017. doi: 10.1002/2017GL074696.
- [21] Zheng Wu, Tom Beucler, Enikő Székely, William T. Ball, and Daniela I. V. Domeisen. Modeling stratospheric polar vortex variation and identifying vortex extremes using explainable machine learning. *Environmental Data Science*, 1:e17, 2022. doi: 10.1017/eds.2022.19.
- [22] Lesley J. Gray, Laura Ferranti, and Adam A. Scaife. Forecasting extreme stratospheric polar vortex events. *Nature Communications*, 11:4630, 2020. doi: 10.1038/s41467-020-18299-7.
- [23] Rachel Wai-Ying Wu, Zheng Wu, and Daniela I. V. Domeisen. Differences in the sub-seasonal predictability of extreme stratospheric events. *Weather and Climate Dynamics*, 3(3):755–776, 2022. doi: 10.5194/wcd-3-755-2022.
- [24] Gaoke Hu, Teng Liu, Maoxin Liu, Wei Chen, and Xiaosong Chen. Condensation of eigen microstate in statistical ensemble and phase transition. *Science China Physics, Mechanics & Astronomy*, 62(9):990511, 2019. doi: 10.1007/s11433-018-9353-x.
- [25] Yu Sun, Gaoke Hu, Yongwen Zhang, Bo Lu, Zhenghui Lu, Jingfang Fan, Xiaoteng Li, Qimin Deng, and Xiaosong Chen. Eigen microstates and their evolutions in complex systems. *Communications in Theoretical Physics*, 73(6):065603, 2021. doi: 10.1088/1572-9494/abf127.
- [26] Yongwen Zhang, Maoxin Liu, Gaoke Hu, Teng Liu, and Xiaosong Chen. Eigen microstates in self-organized criticality. *Physical Review E*, 109(4):044130, 2024. doi: 10.1103/PhysRevE.109.044130.
- [27] Xuan Ma, Rizhou Liang, Xiaosong Chen, Fei Xie, Jinqing Zuo, Cheng Sun, and Ruiqiang Ding. Increased predictability of extreme el niño from decadal interbasin interaction. *Geophysical Research Letters*, 51(23):e2024GL110943, 2024. doi: 10.1029/2024GL110943.
- [28] C. W. J. Granger. Investigating causal relations by econometric models and cross-spectral methods. *Econometrica*, 37(3):424–438, 1969. doi: 10.2307/1912791.
- [29] Jakob Runge, Peer Nowack, Marlene Kretschmer, Seth Flaxman, and Dino Sejdinovic. Inferring causation from time series in earth system sciences. *Nature Communications*, 10(1):2553, 2019. doi: 10.1038/s41467-019-10105-3.

- [30] H. Hersbach, B. Bell, P. Berrisford, G. Biavati, A. Horányi, J. Muñoz Sabater, J. Nicolas, C. Peubey, R. Radu, I. Rozum, D. Schepers, A. Simmons, C. Soci, D. Dee, and J.-N. Thépaut. ERA5 hourly data on pressure levels from 1940 to present, 2023. URL <https://doi.org/10.24381/cds.bd0915c6>.
- [31] Qi Shan and Ke Fan. The transition of stratospheric polar vortex intensity: A case study of winter 1987/88. *Journal of Geophysical Research: Atmospheres*, 127(12): e2022JD036511, 2022. doi: 10.1029/2022JD036511.
- [32] Andrew J. Charlton and Lorenzo M. Polvani. A new look at stratospheric sudden warmings. part i: Climatology and modeling benchmarks. *Journal of Climate*, 20(3):449–469, 2007. doi: 10.1175/JCLI3996.1.
- [33] Wen Chen and Ke Wei. Interannual variability of the winter stratospheric polar vortex in the northern hemisphere and their relations to qbo and enso. *Advances in Atmospheric Sciences*, 26(5):855–863, 2009. doi: 10.1007/s00376-009-8168-6.
- [34] Masaru Inatsu, Naoto Nakano, Seiichiro Kusuoka, and Hitoshi Mukougawa. Predictability of wintertime stratospheric circulation examined using a nonstationary fluctuation–dissipation relation. *Journal of the Atmospheric Sciences*, 72(2):774–786, 2015. doi: 10.1175/JAS-D-14-0088.1.
- [35] Xin Tan and Ming Bao. Linkage between a dominant mode in the lower stratosphere and the western hemisphere circulation pattern. *Geophysical Research Letters*, 47(17):e2020GL090105, 2020. doi: 10.1029/2020GL090105.
- [36] Zheng Wu, Bernat Jiménez-Esteve, Raphaël de Fondeville, Enikő Székely, Guillaume Obozinski, William T. Ball, and Daniela I. V. Domeisen. Emergence of representative signals for sudden stratospheric warmings beyond current predictable lead times. *Weather and Climate Dynamics*, 2:841–865, 2021. doi: 10.5194/wcd-2-841-2021.
- [37] Roberta Quadrelli and John M. Wallace. A simplified linear framework for interpreting patterns of northern hemisphere wintertime climate variability. *Journal of Climate*, 17(19):3728–3744, 2004. doi: 10.1175/1520-0442(2004)017<3728:ASLFFI>2.0.CO;2.